NATURAL SCIENCE REVIEW 3 100704 (2026)
nsr.jinr.int

Temperature-dependent conformational changes of amyloid-β42 in DPPC bilayers

K. A. A. Abdeljawaad*[1,2,3], Y. Arynbek[1,4,5], K. Mamatkulov[1], Huy Le Duc[1,6,7], and G. Arzumanyan[1]

[1] *Joint Institute for Nuclear Research, Dubna, Russia*
[2] *Academy of Scientific Research & Technology (ASRT), Cairo, Egypt*
[3] *Chemistry Department, Faculty of Science, Minia University, Minia, Egypt*
[4] *Faculty of Physics and Technology, al-Farabi Kazakh National University, Almaty, Kazakhstan*
[5] *Institute of Nuclear Physics, Almaty, Kazakhstan*
[6] *Institute of Physics, Vietnam Academy of Science and Technology, Hanoi, Vietnam*
[7] *Graduate University of Science and Technology, Vietnam Academy of Science and Technology, Hanoi, Vietnam*

Abstract

The conformational behavior of the amyloid-β42 (Aβ42) peptide is strongly influenced by the physical state of its surrounding lipid environment. The effect of temperature on the Aβ42 structure within dipalmitoylphosphatidylcholine (DPPC) bilayers was investigated using circular dichroism (CD), Raman spectroscopy, and molecular dynamics (MD) simulations. The study examined two thermal phases: room temperature (RT $= \sim (25 \pm 2)^{\circ}$C), corresponding to the gel phase of DPPC, and $(48 \pm 2)^{\circ}$C, representing the fluid phase above the lipid transition *temperature*. The CD spectroscopy measurements indicated a clear temperature-dependent structural transition of the peptide. At RT, Aβ42 exhibited a conformation enriched in β structures, while at $(48 \pm 2)^{\circ}$C, the spectra revealed a notable increase in α-helical content, reflecting enhanced backbone organization under fluid-phase conditions. Raman spectral analysis supported this trend by demonstrating an increased contribution of α-helical components accompanied by a reduction in β-strand features upon heating. Minor variations in lipid vibrational markers further suggested greater acyl-chain flexibility and bilayer fluidity in the high-temperature state. Furthermore, MD simulations revealed enhanced α-helical content and deeper peptide insertion within the disordered bilayer compared with the ordered gel phase. The findings from experimental and computational investigations demonstrate that membrane fluidization above the DPPC phase transition favors α-helical stabilization of Aβ42, emphasizing temperature as a key parameter governing peptide–lipid conformational equilibria. The results obtained provide a fundamental framework for understanding how thermal conditions modulate amyloid-membrane interactions, which is essential for elucidating the early molecular events associated with amyloid-related pathologies.

Keywords: Amyloid-β42, Raman spectroscopy, circular dichroism, DPPC, molecular dynamics simulation

DOI: 10.54546/NaturalSciRev.100704

*Corresponding author e-mail address: khlood@jinr.ru

Received: 5 March 2026; Revised: 25 May 2026; Accepted: 1 June 2026; Published: 25 June 2026

1. Introduction

The structural variability and misfolding propensity of the amyloid-β (Aβ) peptide are widely recognized as fundamental factors in the onset and progression of Alzheimer's disease [1, 2]. Among the various isoforms derived from amyloid precursor protein processing, the 42-residue Aβ42 species exhibits a pronounced propensity to undergo conformational rearrangements, thereby resulting in self-assembly and fibrillation [3, 4]. The peptide is known to adopt distinct secondary-structure states — α-helical, β-strand, β-turn, and random coil — in response to its physicochemical environment [5]. The aggregation kinetics, membrane affinity and neurotoxicity of the protein are modulated by transitions between these states [6, 7]. Consequently, elucidating how external conditions influence Aβ42 conformation is essential for understanding the molecular events associated with amyloid pathogenesis.

It has been established that biological membranes play a pivotal role in the modulation of Aβ42 structure and aggregation [7]. Interaction with lipid bilayers has been shown to influence the thermodynamic stability of the peptide, as well as its spatial orientation, depth of insertion, and degree of exposure to solvent, as demonstrated experimentally and supported by molecular simulations [8, 9]. Collectively, these factors delineate the peptide's propensity to nucleate oligomeric intermediates or to adopt transient α-helical conformations in membrane-mimicking or helix-promoting environments [10–12]. It has been reported that membrane properties such as lipid composition, head-group charge, and acyl-chain saturation can influence protein–membrane interactions, including those involving Aβ42; however, comparatively less attention has been paid to the physical state of the membrane, particularly its phase properties [13, 14]. DPPC is a model zwitterionic phospholipid frequently employed to investigate peptide–membrane interactions [15]. It exhibits a sharp gel-to-fluid transition at approximately 41°C, providing a well-defined system for examining how bilayer order affects peptide structure [16]. In the lower temperature range, this temperature, the acyl chains adopt an all-trans configuration resulting in a compact, highly ordered gel phase. Above the transition, chain disorder increases, resulting in an expanded area per lipid, enhanced lateral diffusion, and elevated hydration of interfacial regions [15, 17, 18]. Such structural rearrangements modify local polarity and hydrogen-bonding networks, parameters that are known to influence peptide secondary-structure equilibria [19, 20]. Optical spectroscopic techniques are particularly well suited for probing these processes at the molecular level [21–23]. Circular dichroism (CD) spectroscopy provides quantitative information on the global distribution of secondary-structure elements. Characteristic ellipticity minima near 208 and 222 nm correspond to α-helical conformations, while bands around 216–218 nm indicate β-structured regions. Conversely, a pronounced negative band in the far-UV region ($\sim$ 190–200 nm), often centered near 195–200 nm, is typically associated with random coil or disordered structures [24, 25]. Raman spectroscopy, through analysis of the Amide I and Amide III bands, offers complementary sensitivity to backbone hydrogen bonding and side-chain environments while simultaneously reporting on lipid vibrational markers such as the C–C skeletal (1060–1130 cm^{-1}) and CH_2 deformation ($\sim$ 1440 cm^{-1}) modes [21, 26, 27]. The combination of CD and Raman spectroscopy thus provides a multidimensional perspective on how temperature and membrane phase jointly influence peptide and lipid order [21, 24].

The integration of these experimental approaches with molecular dynamics (MD) simulations further strengthens the interpretation by enabling atomistic correlation between spectroscopic observables and structural descriptors [8]. MD simulations are capable of revealing reveal time-resolved information on peptide folding, residue-specific interactions, insertion depth, and

lipid order parameters under varying thermal conditions [9, 28]. Such complementary data allow direct linkage between macroscopic spectral changes and microscopic structural rearrangements, offering a mechanistic understanding unattainable by spectroscopy alone [29]. Previous investigations have established that environmental factors, including solvent polarity, ionic strength, and lipid composition, play a decisive role in shaping Aβ42 conformational equilibria in phospholipid systems. However, the influence of temperature, particularly across the lipid phase transition, remains insufficiently characterized [11, 13]. It is imperative to acknowledge the pivotal yet under-explored role of temperature in the thermodynamic equilibrium between helical and β-structured forms of peptides. This is primarily due to its simultaneous influence on bilayer fluidity and peptide conformational entropy [15, 16]. The present study focuses on the temperature-dependent conformational behavior of Aβ42 in DPPC bilayers by employing CD, Raman spectroscopy, and MD simulations. The investigation focused on two distinct thermal phases: the initial room temperature phase, which is known as the gel phase, and a second phase at $(48 \pm 2)^{\circ}$C, referred to as the fluid phase. The comparative results demonstrate that the transition of the bilayer into the fluid state enhances α-helical stabilization of Aβ42, as evidenced by increased CD ellipticity, strengthened Amide I helical components in Raman spectra, and elevated helical propensity observed in MD trajectories. Collectively, the current findings indicate that membrane fluidization promotes the partial refolding of the peptide into α-helical conformations, while suppressing the increase of formation of other secondary structures (β-turn, rc, β-strand) that are known precursors to β-aggregation. It is imperative to comprehend the manner in which thermal conditions exert their influence on the Aβ42 structure within lipid membranes, as this engenders a profound comprehension of the fundamental physicochemical principles that govern amyloid behavior within biological environments. This knowledge contributes to the broader framework of temperature- and membrane-regulated protein misfolding, offering potential implications for the design of experimental models and therapeutic strategies targeting the early stages of amyloid formation.

2. Materials and methods

2.1. Sample preparation

Liposomes were prepared from 1,2-dipalmitoyl-sn-glycero-3-phosphocholine (DPPC) (Avanti Polar Lipids, USA; catalog no. 850355P-500mg, lot no. 850355P-500MG-A-325) using the electroformation method. DPPC was dissolved in chloroform (Sigma-Aldrich, USA; catalog no. 650498-1L, lot no. MKCX6071) at a concentration of 16.8 mg/mL. An aliquot (17 μL) of the lipid solution was spread dropwise onto the conductive side of an indium tin oxide (ITO)-coated glass slide and allowed to dry at ambient pressure for 60 min to form a homogeneous lipid film. A 16 mm silicone O-ring (chemically inert under experimental conditions) was placed around the lipid film, which was subsequently rehydrated with 300 μL of buffer solution (150 mM NaCl, 10 mM Tris-HCl, pH 7.4). The assembly was mounted in the electroformation chamber (Vesicle Prep Pro, Nanion Technologies GmbH, Germany), sealed with a second ITO-coated slide, and subjected to an alternating electric field (3 V, 5 Hz) for 60 min at 45°C. This temperature, slightly above the main phase transition temperature of DPPC ($\sim$ 41°C), ensures bilayer fluidity and promotes vesicle formation. The resulting liposomes were collected and used without further modification.

The Aβ42 peptide (Cloud-Clone Corp., China; catalog no. SPA946Hu02, lot no. P20251103001, purity $>$ 95%) was obtained in lyophilized powder form and dissolved in phosphate-buffered saline (PBS, pH 7.4) to a final concentration of 40 μM. The solution was

freshly prepared immediately prior to use without additional monomerization treatment in order to minimize time-dependent aggregation effects. For preparation of the Aβ42–DPPC hybrid system, the peptide was incorporated as an aqueous solution during the electroformation process. Specifically, 180 μL of the freshly prepared peptide solution was used to rehydrate the dry lipid film on the ITO slide, ensuring homogeneous distribution within the forming lipid vesicles. The final concentrations were approximately 1.29 mM ($\approx$ 0.95 mg/mL) for DPPC and 40 μM for Aβ42, corresponding to $\sim$ 3 mol% peptide relative to lipid. These sample preparations were used for both Raman spectroscopy and circular dichroism (CD) measurements. The prepared Aβ42–DPPC systems were equilibrated at $\sim (25 \pm 2)^{\circ}$C and $\sim (48 \pm 2)^{\circ}$C, corresponding to the gel and fluid phases of DPPC, respectively, prior to spectroscopic analyses.

2.2. Raman spectroscopy

Raman spectra were acquired using a Confotec MR 200 confocal Raman microscope (SOL Instruments, Minsk, Belarus) in order to evaluate the influence of conditions above and below the lipid phase-transition temperature influence the secondary structure of Aβ42–DPPC systems. Excitation was provided by a 633-nm laser focused onto the sample with a $\times$ 50 objective (NA = 0.60), yielding an approximate 1 μm spot size. The backscattered light collected through the objective was directed to a 150 mm focal-length grating monochromator-spectrograph equipped with a 600 grooves mm^{-1} grating. A cooled 2048 $\times$ 64-element CCD array served as the detector. For each measurement, 5 μL of the sample was deposited on a clean microscope slide, which was then positioned on the motorized stage. Spectra were recorded from 930 to 1800 cm^{-1} with an acquisition time of 20 s per spectrum. Each condition was measured at least five times using freshly deposited drops from the same prepared sample, and the resulting spectra were averaged and smoothed using a 7-point Savitzky–Golay filter with a polynomial order of 2. The Amide I region was then deconvolved and fitted with six to eight Gaussian components using OriginPro 2021 (v9.1). The number of Gaussian components (six to eight) was selected based on the spectral complexity and optimized by incrementally increasing the number of components until no significant improvement in the fit quality (as assessed by residuals) was observed, while avoiding overfitting. All spectroscopic experiments were performed in saline buffer solution containing 10 mM Tris-HCl (pH 7.4) and 150 mM NaCl. The temperature was maintained at room temperature (RT, around $(25 \pm 2)^{\circ}$C) and precisely maintained at $(48 \pm 2)^{\circ}$C using a LTS120 temperature-controlled stage (Linkam Scientific Instruments Ltd., United Kingdom).

2.3. Circular dichroism

CD spectra were captured using a MOS-500 spectropolarimeter (Bio-Logic, France). Measurements were performed in an optical UV-grade quartz cuvette with a path length of 0.5 mm (PIKE Technologies, USA) suitable for far-UV measurements. Spectra were recorded over the range of 190 to 250 nm with a 0.5 nm intervals, with a scanning speed of 30 nm per minute, a time per point of 2.0 s, and a bandwidth of 2 nm. Each final spectrum represented the average of five accumulations obtained under identical conditions to improve the signal-to-noise ratio. The Aβ42–DPPC samples were prepared in 10 mM sodium phosphate buffer solution at a pH of 7.4 to maintain a neutral environment. CD measurements were performed at two temperatures: room temperature ($\approx (25 \pm 2)^{\circ}$C), which corresponds to the gel phase of DPPC, and $(48 \pm 2)^{\circ}$C, representing the fluid phase above the main transition temperature of the lipids. Samples were thermally equilibrated for 1 h prior to each measurement to ensure temperature stability. To correct for background contributions, the CD spectra were recorded of DPPC-only liposomes

(without peptide) and used as reference baselines for subtraction. The resulting spectra of the Aβ42–DPPC system were then converted to mean residue ellipticity $[\theta]$ in deg $\cdot$ cm^2 $\cdot$ dmol^{-1} to normalize for differences in peptide concentration and optical path length. The estimation of the secondary-structure composition of Aβ42 was then performed using the CDPro software package, which integrates the SELCON3 [30], CONTIN/LL [31], and CDSSTR algorithms [32]. The averaged spectra were analyzed using the SP175 reference dataset to provide a quantitative assessment of the α-helix, β-sheet, turn, and unordered random coil (RC) components.

2.4. Molecular dynamics simulations

A series of molecular dynamics (MD) simulations were performed with the objective of providing atomic-level insight into the temperature-dependent conformational transitions of Aβ42 in DPPC bilayers. The initial configurations were prepared using the CHARMM-GUI Membrane Builder platform [33], which facilitates accurate construction of heterogeneous biomolecular assemblies containing lipids, peptide, water and ions. The NMR-derived structure of Aβ42 (PDB ID: 1Z0Q) [34] was selected as the starting peptide conformation. The protonation states of all ionizable amino acid residues were assigned to correspond to physiological pH 7.4. Standard protonation states were assumed (ASP and GLU deprotonated; LYS and ARG protonated), while histidine residues were modeled in their neutral form based on local hydrogen-bonding considerations. A symmetric DPPC bilayer with a composition of 56 lipids on each side was constructed to represent a membrane model that is well-hydrated and structurally stable. Lipid parameters for DPPC were obtained from the CHARMM36 lipid force field, as implemented in the CHARMM-GUI Membrane Builder, ensuring full compatibility with the CHARMM36m protein parameters. This model is frequently employed in studies of peptide–lipid interaction. The initial positioning of Aβ42 within the bilayer was performed using the membrane insertion protocol of CHARMM-GUI, without the use of external bioinformatics prediction tools. The peptide was oriented such that its hydrophobic C-terminal segment was embedded within the hydrophobic core of the bilayer, while the N-terminal residues remained exposed to the aqueous phase. The peptide center of mass was aligned near the lipid-water interface, enabling partial insertion consistent with experimentally observed membrane-associated conformations of Aβ42. This approach was designed to minimize steric overlaps and enable natural lipid rearrangement around the peptide. Prior to the insertion of the peptides, the bilayer underwent a process of pre-equilibration with the objective of attaining uniform area per lipid and lateral packing. Subsequently, the system was solvated with explicit TIP3P water molecules [35] and neutralized to a physiological ionic strength of 0.15 M NaCl. All atomic interactions were described using the CHARMM36m force field [36] for both the peptide and DPPC lipids to ensure parameter consistency. While this potential function exhibits a slight preference for α-helical over β-sheet conformations, it has been extensively validated for simulations of amyloid peptide in lipid environments [37]. Subsequently, the complete systems were simulated using GROMACS version 2024.3 [38]. The energy minimization process was initially executed using the steepest-descent algorithm (5000 steps) to eliminate unfavorable contacts. Subsequent equilibration was performed in two stages: (*i*) NVT equilibration for 500 ps using the V-rescale thermostat to stabilize the temperature distribution, and (*ii*) NPT equilibration for 2 ns under semi-isotropic pressure coupling (1 bar) via the Parrinello–Rahman barostat [39]. Initial atomic velocities were assigned according to a Maxwell–Boltzmann distribution at the target simulation temperatures (298 and 321 K) at the start of each equilibration phase. The production simulations were then executed for 200 ns in the NPT ensemble at two temperature conditions: 298 K (gel phase) and 321 K (fluid phase), they are consistent with the experimental conditions em-

ployed in the CD and Raman experiments. For each temperature condition, three independent simulations were performed. The Nosé–Hoover thermostat was utilized to maintain temperature with a 1-ps relaxation time, and the Parrinello–Rahman barostat was employed to control pressure with a 5-ps coupling constant. The application of periodic boundary conditions was implemented in all three dimensions. The long-range electrostatic interactions were treated with the Particle Mesh Ewald (PME) algorithm [40], while van der Waals interactions were truncated at 1.2 nm. The LINCS algorithm was used to constrain bonds thereby involving hydrogen atoms, enabling a 2-fs integration time step. Trajectory analyses were conducted utilizing Visual Molecular Dynamics (VMD) [41]. A range of additional descriptors were extracted from the trajectory files, including root-mean-square deviation (RMSD) and hydrogen bond numbers. Hydrogen bond analysis was performed using the hydrogen bond plugin implemented in VMD and was defined based on geometric criteria, with a donor–acceptor distance cutoff of 3.5 Å and a hydrogen-donor–acceptor angle cutoff of 30°. Both intra-peptide and peptide–lipid hydrogen bonds were computed over the trajectory, and time-dependent hydrogen bond counts were used to evaluate stability and fluctuations. Secondary structure kinetics were analyzed using the Timeline plugin in VMD, which assigns secondary structure based on backbone geometry and hydrogen-bonding patterns. Time-resolved secondary structure profiles were generated to monitor the evolution of α-helical and β-structure content throughout the simulations.

3. Results and discussion

3.1. Raman spectroscopy

Raman spectroscopy was utilized to examine the temperature-dependent structural behavior of the Aβ42–DPPC system. This vibrational technique is widely recognized for its exceptional sensitivity to molecular conformation, enabling precise detection of structural changes in biological macromolecules under varying environmental conditions. In order to illustrate the spectral variations induced by temperature, Figure 1 presents the Raman spectra of the Aβ42–DPPC system, along with the corresponding secondary structure assignments in the Amide I region, measured at room temperature (RT) and (48 ± 2)°C.

The spectra of Aβ42–DPPC are dominated by characteristic lipid vibrational modes in the region of 1000 to 1500 cm^{-1}. It is first important to note that the Raman modes between 1025 and 1150 cm^{-1} are assigned to the skeletal hydrocarbon chain C–C stretching vibrations of phospholipids, which are largely absent in the Aβ42–PBS spectrum, Figure 1, *a*. This region includes the bands at 1062 and 1125 cm^{-1}, which are identified as key markers of the symmetric and asymmetric stretching vibrations of the carbon atoms, respectively [42]. These vibrations are associated with trans conformations. In addition, the peak observed at 1088 cm^{-1} is the result of a superposition of the C–C modes of the hydrocarbon portions containing gauche bonds and the symmetric PO_2^--stretching vibration [43, 44]. This phenomenon is attributed to the sensitivity of these vibrations to a single gauche defect and/or the formation of multiple gauche structures [45, 46].

It is evident that as the temperature increases, there is a concomitant rise in the relative abundance of gauche conformers compared to trans conformers. This phenomenon can be attributed to the transition of the solvent from a gel state at room temperature to a more liquid-crystalline state at elevated temperatures. In the gel phase, the acyl chains exhibit a high packing density characterized predominantly by all-trans configurations, with only a minimal presence of gauche bonds. As the phase transition temperature (T_m) is approached,

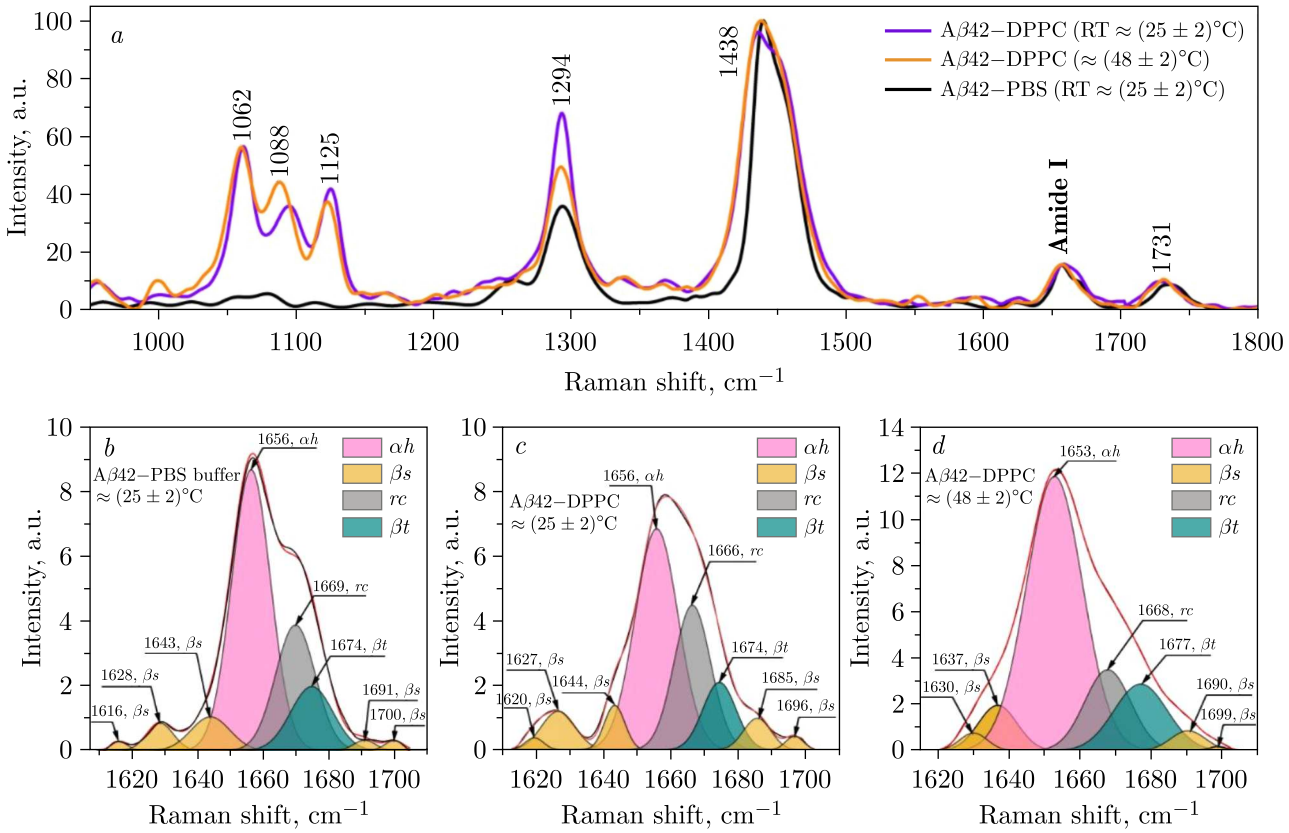

Figure 1. *a*) Raman spectra of the Aβ42–DPPC system at RT ((25 ± 2)°C, violet line), (48 ± 2)°C (orange line), and Aβ42 in PBS in the absence of DPPC at (25 ± 2)°C (black line). Deconvoluted Raman spectra in the Amide I region of Aβ42: Aβ42 in PBS at (25 ± 2)°C (*b*), Aβ42–DPPC at (25 ± 2)°C (*c*), and Aβ42–DPPC at (48 ± 2)°C (*d*). Red line — fitted curve, filled areas — deconvolved spectra by Gaussian function. αh — α-helix (in pink), rc — random coil (in gray), βt — β-turn (in dark cyan), and βs — β-strand (in yellow).

approximately 41°C, the lipid film undergoes a transition to the liquid-crystalline phase [47]. This transition is accompanied by a conformational rearrangement of the acyl chains, shifting from predominantly all-trans configurations towards those containing a greater proportion of gauche "elbows". This structural change results in enhanced band intensity and a noticeable peak shift in the Raman spectra. Concurrently, Aβ42 engages with the membrane, penetrating the hydrophobic core of the fluid phase and thereby increasing chain disorder. This interaction promotes the formation of additional gauche bonds and to further amplify the Raman signal at elevated temperatures [48, 49]. The substantial increase in gauche conformers observed at higher temperatures ($> T_m$) thus provides strong evidence for the occurrence of a phase transition within the system under investigation [50].

Turning to the Raman spectra in the amide region, specifically the Amide III band, typically observed between 1200 and 1350 cm^{-1}, the band at 1294 cm^{-1} is present in all three spectra, as shown in Figure 1, *a*. However, this mode corresponds to the Amide III in the pure peptide, whereas in the DPPC-containing samples, it primarily arises from lipid CH_2 twisting vibrations, resulting in a strong overlapping signal that confirms peptide–membrane association [51]. This band lies directly within the Amide III region and almost completely masks any weak contributions from Aβ42 in this spectral range, as also noted in the literature [52].

Additional lipid markers include the CH_2 scissoring mode at 1438 cm^{-1} and the ester carbonyl (C = O) stretching vibration at 1731 cm^{-1}.

Therefore, the present study focuses on the analysis of the Amide I band, which typically ranges from 1610 to 1720 cm^{-1}. This region distinctly reflects the bonding interactions between carbonyl and amide groups within the Aβ42–DPPC system [37, 53, 54]. Among the amide bands, Amide I is widely regarded as the most direct and accurate marker of protein secondary structure, outperforming Amide II and Amide III. This band is highly sensitive to temperature-induced conformational changes in proteins. The Amide I region is dominated by the C = O stretching vibration, which is particularly responsive to secondary structure because the carbonyl group directly participates in N–H hydrogen bonding networks. These hydrogen-bonding patterns differ systematically among various secondary structure elements, including αh, βs, βt, and disordered conformations. As a result, any alteration in the hydrogen-bonding environment of the C = O group leads to a corresponding shift or change in the Amide I signal, making it an exceptionally reliable probe for monitoring secondary structure rearrangements [55, 56]. The results obtained demonstrate clear alterations in frequency and spectral shape, exhibiting high sensitivity to the secondary structure of the Aβ peptide in response to thermal denaturation, consistent with the findings of Lin et al. [57]. Raman spectra were collected from samples containing Aβ42–DPPC systems in saline buffers at both room and elevated temperature. In order to monitor variations in intensity and peak positions within the Amide I band, as illustrated in Figure 1, *b–d*, spectral deconvolution was performed. The deconvolved Raman spectra were then fitted using Gaussian functions to determine the relative contributions of each secondary structure. This is a critical step in elucidating the kinetics of Aβ42 conformational transitions. The Raman spectral analysis revealed that the most intense peak, located between 1650 and 1660 cm^{-1}, corresponds to the α-helix structure [58]. Peaks in the regions 1615–1645 cm^{-1} and 1687–1700 cm^{-1} are assigned to the β-strand structure, whereas those at 1660–1670 cm^{-1} and 1670–1680 cm^{-1} are attributed to random coil and β-turn structures, respectively [59, 60]. To contribute to research efforts aimed at inhibiting Aβ42 aggregation, emphasis was placed on evaluating the integrated areas under the deconvoluted peaks corresponding to the spectral weight of the secondary structures (αh, rc, βt, and βs). This analysis provides valuable insights into conformational dynamics and establishes a foundation for developing potential anti-aggregation strategies.

Raman spectroscopy was also employed to provide complementary structural information. Within the Amide I region, both spectra at RT and (48 ± 2)°C exhibited a predominance of αh structures. Conversely, rc emerged as the second most abundant component, while β-structures remained at the lowest levels. At approximately (25 ± 2)°C, the αh component (at 1656 cm^{-1}) accounted for nearly half of the total, with 46%, while the rc component (at 1666 cm^{-1}) contributed 25.7%. The βt structure (at 1674 cm^{-1}) represented 10.9%, and the βs components (at 1620, 1627, 1644, and 1696 cm^{-1}, respectively) collectively contributed 17.4%. DPPC is capable of forming a hydrophobic bilayer with a polar headgroup region [61]. When Aβ42 is incorporated into the DPPC bilayer structure, its N-terminal residues interact electrostatically with the phosphocholine headgroups, while the hydrophobic C-terminal domain inserts into the acyl-chain region [62]. This interfacial insertion stabilizes the αh segments by shielding the peptide backbone from water, thereby promoting intra-chain hydrogen bonding over inter-chain interactions. Consequently, the lipid environment is conducive to the αh conformation [3]. This trend aligns closely with the overall conformational distribution profile of Aβ42 in the PBS-only system, wherein αh (at 1656 cm^{-1}) and rc (at 1669 cm^{-1}) structures constitute the predominant populations at 51.3% and 23.5%, respectively, while β-structure

conformations remain minimally represented (12.7% for βt at 1674 cm^{-1} and a total of 12.5% for βs at 1616, 1628, 1643, 1691, and 1700 cm^{-1}, respectively). In contrast, the lipid–peptide assembly exhibits a notable shift in secondary structural states. The βs contribution increases from 12.5% to 17.4%, along with a reduction in αh from 51.3% to 46.0%. This redistribution suggests that interactions between Aβ42 and DPPC lipids promote a partial conformational reorganization toward β-enriched states. However, βs populations remaining below the 20% threshold imply that this lipid-induced structural modulation does not drive the peptide toward complete amyloid fibrillization.

At ambient temperature, DPPC remains in the gel phase, in which the lipid bilayer exhibits enhanced order and tight packing, thus influencing the changing secondary structures of the peptide. This directly influences the formation of βs in Aβ42, as β-structure development requires sufficient peptide–peptide hydrogen bonding and proper β-strand alignment. The formation of rc regions is attributable to residues that fail to attain a stable environment. Residues located at the interface between hydrophilic headgroups and hydrophobic tails experience heterogeneous polarity and fluctuating hydrogen bonding, remaining partially unfolded or flexible and thus contributing to the observed rc signal.

At elevated temperatures ((48 ± 2)°C), immediately following the phase transition of DPPC from the gel to the liquid-crystalline phase, the DPPC environment becomes softer and more dynamic. This transition exerts a significant influence on the secondary structure of the Aβ42 chain [63]. As the viscosity of the lipid matrix decreases, and the αh component (at 1653 cm^{-1}) increases up to 60%, the hydrophobic peptide segments can more readily insert into the DPPC acyl core — an energetically favorable hydrophobic environment, thereby reinforcing intra-chain hydrogen bonding. In a more flexible lipid environment, acyl chains exhibit enhanced thermal motion, creating space for Aβ42 to rearrange and fold into stable helical segments [64]. Conversely, the rc structure (at 1668 cm^{-1}), which is conventionally linked to peptide–water interactions and conformational flexibility, exhibits a decline to 14.5%. This reduction is attributed to the predominance of more ordered αh configurations. In summary, DPPC liquefaction reduces peptide–water exposure, therby enabling rc segments to convert into helices as a means of minimizing free energy through intra-chain hydrogen bonding. With regard to the βs structures (at 1630, 1637, 1690, and 1699 cm^{-1}), a decline to 11.9% was observed, which is likely to be due to disruption of inter-chain hydrogen bonds that stabilize β-sheets. In addition, within the liquid-crystalline phase, Aβ42 molecules exhibit increased dispersion and reduced direct peptide–peptide interactions, thereby constraining β-sheet formation. The βt content (at 1677 cm^{-1}) exhibited a marginal increase to 13.8%, suggesting enhanced local flexibility of the polypeptide chain, as short segments bend to connect helical and coil regions. When βs structures are decreased by heat of the system, peptide segments do not fully revert to rc configurations; instead, they form transient βt fragments that help stabilize the overall structure. Comprehensively, the Aβ42–DPPC system demonstrates a "restructuring" state at (48 ± 2)°C, characterized by enhanced αh growth and a reduction in rc content in the liquid-crystalline phase. Concurrently, the loss of stability in βs may be due to rupture of inter-chain hydrogen bonds [65], along with increased βt flexibility, reflecting a dynamic equilibrium between structural order and flexibility of the peptide within the biological membrane. This equilibrium underscores the protective role of lipids in stabilizing the helical conformation and preventing the conversion of Aβ42 to β-chains, which then proceed to β-aggregates and cytotoxic states.

3.2. Circular dichroism

Circular dichroism spectroscopy was employed as the primary investigative method to observe and document temperature-induced alterations in the secondary structure of Aβ42 within DPPC bilayers. Figure 2 displays the CD spectra of the Aβ42–DPPC system recorded at two distinct thermal conditions: RT and (48 ± 2)°C, corresponding to the gel and fluid phases of DPPC, respectively. For comparison, the CD spectrum of Aβ42 in PBS buffer at (25 ± 2)°C in the absence of DPPC was also included as a reference state for evaluating membrane-induced conformational changes. At room temperature (RT), the CD spectrum of the Aβ42–DPPC complex exhibited a dominant negative band in the 190–200 nm region, indicative of a predominantly disordered or random-coil conformation of the peptide. The relatively high α-helical content observed at (25 ± 2)°C differs from that typically reported for Aβ42 in aqueous solution. However, it is well established that membrane environments can stabilize α-helical conformations of amphipathic peptides due to hydrophobic interactions and reduced solvent exposure. Therefore, even in the gel phase of DPPC, partial membrane association may promote helix formation. This observation suggests that, within the ordered gel-phase bilayer, the peptide remains predominantly unfolded and lacks a defined secondary structure. As the temperature was elevated to (48 ± 2)°C, corresponding to the fluid phase of DPPC, a marked change in the CD spectrum was observed, with the emergence of features typical of α-helical organization and an overall increase in negative ellipticity. These spectral changes indicate that the enhanced lipid fluidity and interfacial hydration at elevated temperatures facilitate partial folding of Aβ42 into α-helical conformations. The control spectra of pure DPPC vesicles at both temperatures exhibited negligible ellipticity, confirming that the observed signals originated from the peptide rather than the lipid component. The spectral evolution reflects the strong coupling between peptide conformation and the physical state of the membrane. When DPPC undergoes a gel-to-liquid-crystalline transition above its main transition temperature, the increased chain mobility and interfacial hydration provide a more flexible environment that supports intramolecular hydrogen-bond formation. This, in turn, stabizes helical structures and diminishes β-aggregation tendencies.

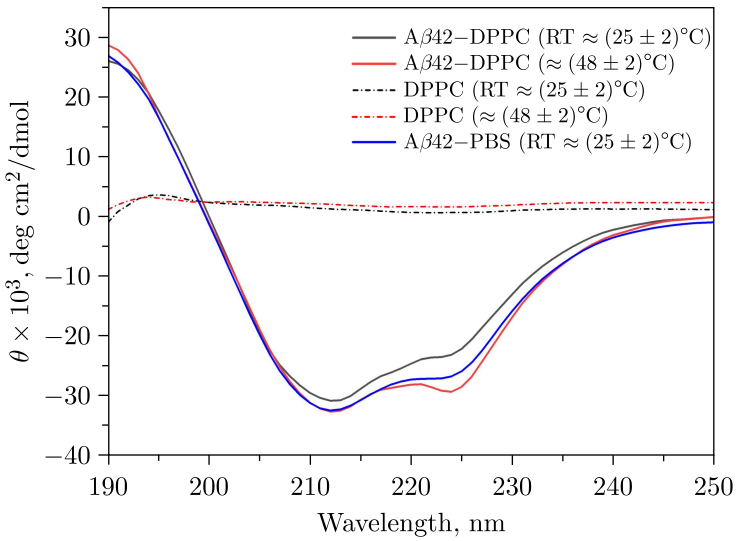

Figure 2. CD spectra of the Aβ42–DPPC complex recorded at (25 ± 2)°C (in black) and (48 ± 2)°C (in red). For comparison, the spectra of DPPC-only samples and Aβ42 in PBS buffer at (25 ± 2)°C are also presented.

Table 1. Percentage contribution of α-helix, β-strand, β-turn, and random coil elements of Aβ42 at different temperatures according to the Raman, CD, and MD simulations outcomes.

Secondary structure	Room temperature ((25 ± 2)°C)			High temperature ((48 ± 2)°C)		
	Raman	CD	MD	Raman	CD	MD
α-helix	46.0 ± 2	44.9 ± 3	42.1	59.8 ± 2.5	58.2 ± 3.5	64.0
β-strand	17.4 ± 3	9.7 ± 4	0.0	11.9 ± 4	9.9 ± 5	0.0
β-turn	10.9 ± 2	17.9 ± 3	41.4	13.8 ± 2.5	10.4 ± 3.5	15.3
Random coil	25.7 ± 2.5	29.2 ± 3.5	15.2	14.5 ± 3	22.5 ± 3.5	20.2

Furthermore, the quantitative analysis of the spectra using the CDPro package (SELCON3, CONTIN/LL, and CDSSTR algorithms) verified this trend. Quantitative analysis of the CD spectrum of Aβ42 alone revealed a secondary-structure composition of 50.8% α-helix, 12.3% β-strand, 11.9% β-turn, and 23.2% random coil. As summarized in Table 1, at (25 ± 2)°C the secondary structure of Aβ42 consisted of approximately 44.9% α-helix, 9.7% β-strand, 17.9% β-turn, and 29.2% random coil. Upon increasing the temperature to (48 ± 2)°C, the α-helical content increased to 58.2%, accompanied by a reduction in β-turn (10.4%) and random coil (22.5%) contributions, while the β-strand content remained nearly unchanged (9.9%). This temperature-dependent redistribution of secondary-structure components highlights the role of membrane fluidization in promoting peptide refolding toward a more ordered, α-helical state. Moreover, the normalized root-mean-square deviation (NRMSD) values were low (0.051 at 25°C and 0.049 at 48°C), indicating good agreement between experimental and reconstructed spectra. The conformational behavior observed in the present study is consistent with previous reports demonstrating the strong environmental sensitivity of Aβ42 secondary structure. Earlier CD investigations have shown that Aβ peptides in aqueous solution predominantly adopt random-coil or β-structured conformations, whereas membrane-mimicking environments and lipid interfaces can stabilize α-helical states depending on lipid composition, peptide concentration, and membrane fluidity [66]. In particular, comparable α-helical spectral characteristics have been reported for Aβ under conditions promoting peptide-membrane interactions or altered local environments [67, 68]. However, unlike previous studies primarily focused on lipid composition or peptide aggregation, the present work specifically demonstrates the influence of the DPPC phase transition itself on the conformational equilibrium of membrane-associated Aβ42. The observed increase in α-helical content upon transition from the gel to fluid phase highlights membrane fluidization as an important regulator of peptide structural organization. Overall, these results demonstrate that thermal modulation of the bilayer not only alters lipid packing but also acts as a structural determinant for membrane-bound Aβ42, favoring conformations that are less prone to aggregation.

3.3. Molecular dynamics simulations

Molecular dynamics (MD) simulations were performed to provide atomistic insight into the temperature-dependent conformational behavior of Aβ42 within DPPC bilayers and to complement the experimental observations obtained from Raman and CD spectroscopy. The simulations facilitate direct visualization of peptide dynamics, membrane insertion, and intramolecular stabilization mechanisms that are not resolvable through experimental means. The initial structure of Aβ42 used for the simulations exhibited the following secondary-structure composition: 59.52% α-helix, 21.42% random coil, and 19.04% β-turn. Figure 3 shows the time evolution

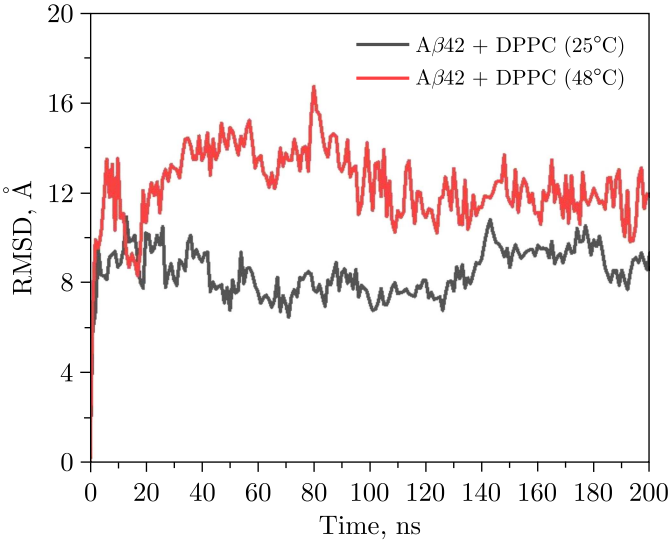

Figure 3. RMSD of Aβ42 embedded in a DPPC bilayer at 25°C (in black) and 48°C (in red) over 200 ns of MD simulations.

of the root-mean-square deviation (RMSD) of the Aβ42 backbone at both temperatures over the 200-ns trajectories. At room temperature (25°C), the RMSD rapidly increased during the initial equilibration phase and fluctuated around higher values throughout the simulation. This indicated the significant conformational instability and structural rearrangements of the peptide in the ordered gel-phase membrane. These fluctuations are indicative of the restricted mobility and rigid lipid packing of DPPC below its main transition temperature, which limits the ability of the peptide to adopt a stable folded state. Conversely, at elevated temperature (48°C), the RMSD values attained a plateau earlier and remained comparatively lower and more stable during the production run. This behavior suggests that Aβ42 rapidly attains a more equilibrated and conformationally stable structure within the fluid-phase bilayer. The reduced RMSD fluctuations at elevated temperatures indicate a constrained structural ensemble characterized by persistent secondary structural elements, which is consistent with the augmented α-helical content observed in the experimental studies by CD and Raman spectroscopy.

Further insight into peptide stabilization was obtained by analyzing the number of intramolecular hydrogen bonds formed within Aβ42 during the course of the simulations (Figure 4). At (25 ± 2)°C, the peptide demonstrated a reduced and more variable number of hydrogen bonds, indicative of the prevalence of disordered and transient conformations. In the gel-phase membrane, the restricted lipid dynamics hinder efficient peptide insertion and folding, thereby limiting the formation of stable intra-chain hydrogen bonding patterns. Conversely, at (48 ± 2)°C, a significant increase in the average number of hydrogen bonds was observed, accompanied by reduced temporal fluctuations. This increase indicates the formation of persistent hydrogen-bond networks, which are characteristic of α-helical structures. The fluid DPPC bilayer provides a more accommodating hydrophobic environment that promotes backbone desolvation and facilitates intra-chain hydrogen bonding, thereby stabilizing helical segments and reduces the peptide exposure to the aqueous phase.

The secondary-structure evolution of Aβ42 over the simulation time was further quantified, as depicted in Figure 5. At 25°C (Figure 5, *a*), the peptide displayed a heterogeneous structural profile dominated by random coil and β-turn elements, with only short and unstable α-helical fragments. These transient helices frequently unfolded, reflecting the inability of the

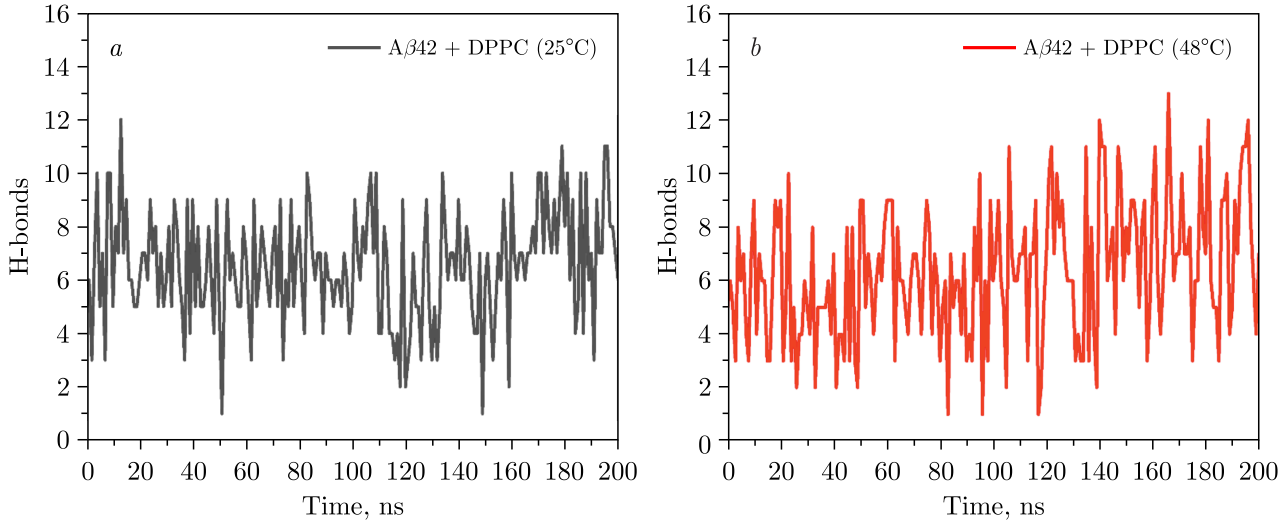

Figure 4. Number of hydrogen bonds formed by Aβ42 in a DPPC bilayer at 25°C (in black) (*a*) and 48°C (in red) (*b*) over 200 ns of MD simulations.

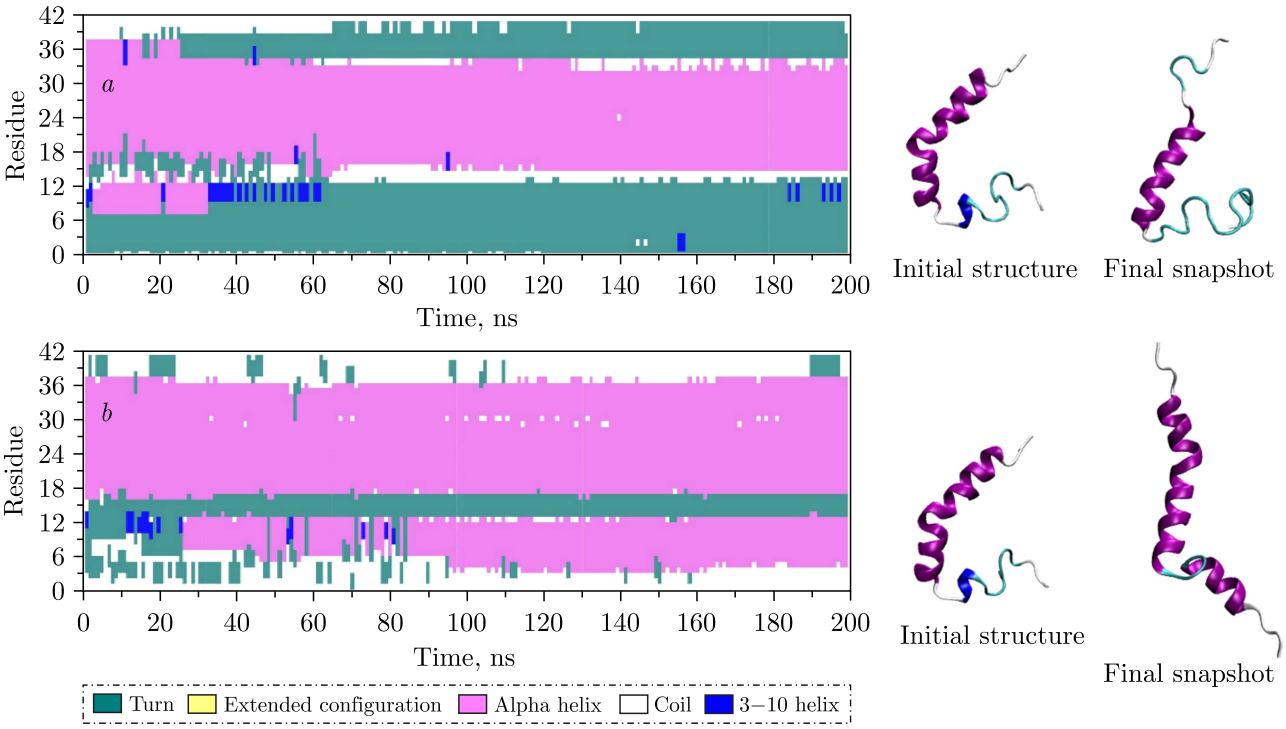

Figure 5. Temperature-dependent secondary structure dynamics of Aβ42 in a DPPC lipid environment: 25°C (*a*) and 48°C (*b*). Initial and final structures are shown on the right.

rigid lipid environment to support sustained secondary structure formation. Conversely, at elevated temperatures (see Figure 5, *b*), the peptide demonstrated a significant enrichment of α-helical content across substantial segments of its sequence, particularly within the central and C-terminal hydrophobic regions. These helical segments persisted for extended time intervals, indicating long-lived conformational stability. The reduction in β-structure and random coil populations at elevated temperature is in excellent agreement with both Raman deconvolution and CDPro analysis, which independently demonstrated an increase in α-helical content and

a concomitant decrease in disordered structures. Structurally, the simulations revealed that at (48 ± 2)°C Aβ42 penetrates deeper into the disordered acyl-chain region of the DPPC bilayer compared to its position at (25 ± 2)°C, where it remains primarily localized near the lipid headgroup interface. This deeper insertion at elevated temperatures has been shown to shield hydrophobic residues from water, reduce backbone solvation, and energetically favor intramolecular hydrogen bonding over inter-molecular interactions. Such conditions are optimal for stabilizing α-helical conformations and disfavoring β-sheet formation, which typically requires peptide–peptide alignment and exposure to aqueous environments.

The MD simulations collectively provide a mechanistic explanation for the experimental observations. Membrane fluidization above the DPPC phase transition enhances lipid disorder and interfacial flexibility, enabling Aβ42 to insert more deeply into the bilayer and reorganize into a stable α-helical conformation. In contrast, the rigid gel-phase membrane restricts peptide mobility and promotes conformational heterogeneity with a preponderance of random coil and β-type structures. These findings provide substantial evidence that supports the conclusion that temperature-dependent membrane dynamics act as a critical regulator of amyloid secondary structure. It is hypothesised that membrane dynamics may play a protective role by suppressing β-sheet-rich, aggregation-prone states associated with amyloid toxicity.

3.4. Methodological consistency across spectroscopic and simulation data

As illustrated in Table 1, a direct comparison of the secondary structure estimates obtained from Raman spectroscopy, circular dichroism, and molecular dynamics simulations under different thermal conditions is enabled. In general, the three approaches demonstrate a high degree of qualitative agreement in identifying α-helical structures as the predominant conformational motif of Aβ42 at both room and elevated temperatures. At approximately (25 ± 2)°C, all methods indicate substantial α-helical content, although quantitative differences are evident. Raman and CD yield comparable values ($\sim 45\%$), whereas MD simulations predict a slightly lower α-helical contribution accompanied by a markedly higher proportion of β-turn structures. It is important to note that β-strand elements have been identified through the use of both spectroscopic techniques. However, these elements are not present in the MD-derived ensemble, which indicates a systematic discrepancy between the experimental and computational representations of extended β-structures. At (48 ± 2)°C, convergence between the methods becomes more pronounced with respect to α-helical content, with all techniques reporting values exceeding 58%. This finding suggests that thermal effects are reliably measured across a range of experimental and simulation frameworks. Conversely, the relative contributions of β-turn and random coil conformations remain method-dependent. The results of MD simulations indicate a substantial redistribution from β-turn structures to α-helical states. In contrast, Raman and CD measurements reveal higher levels of structural disorder. These disparities are presumably attributable to the discrete physical underpinnings inherent to each method. Spectroscopic techniques probe ensemble-averaged conformations in real experimental environments, whereas MD simulations are constrained by force field parameterization and sampling timescales. However, the consistent alignment of major trends across various studies lends credence to the use of a combined approach involving Raman, CD, and MD as complementary tools for investigating peptide conformational dynamics.

It also worth noting that a previous study have demonstrated that Aβ42 adopts α-helical conformations in fluorinated alcohols, where two helical segments (residues 8–25 and 28–38) connected by a β-turn were identified by NMR analysis [12]. This highlights the strong environmental sensitivity of Aβ42 structure. In the present system, a similar increase in α-helical

content is observed; however, the underlying mechanism is fundamentally different, arising from interactions with the DPPC lipid bilayer rather than solvent-induced effects.

4. Conclusion

The present investigation provides an integrated spectroscopic and computational perspective on how temperature modulates the structural organization of the amyloid-β42 peptide within phospholipid membranes. The collective analysis of circular dichroism and Raman spectroscopy collectively demonstrated that the conversion of dipalmitoylphosphatidylcholine (DPPC) from the gel to the fluid phase induced a measurable shift in the secondary-structure equilibrium of Aβ42 towards α-helical conformations. This behavior contrasts with the β-aggregation typically observed in aqueous environments, indicating that enhanced bilayer fluidity stabilizes amphipathic helical states at the membrane interface. The results of MD simulations corroborated these experimental findings, thereby demonstrating increased helical propensity, deeper peptide insertion, and reduced interfacial disorder in the fluid phase in comparison with the ordered gel state. The correlation between experimental and computational data highlights the cooperative relationship between lipid dynamics and peptide folding. The results of this study underscore the pivotal regulatory function of the membrane's thermal state on amyloid structure, thereby establishing a nexus between bilayer phase behavior and the conformational landscape of Aβ42. The recognition of this coupling provides a deeper understanding of the physicochemical mechanisms governing amyloid-membrane interactions and offers a framework for interpreting temperature-dependent aggregation phenomena observed in neuronal membranes. It is suggested that future work extending this approach to heterogeneous lipid mixtures and longer timescale simulations may further elucidate how local membrane composition and thermal fluctuations influence the early molecular events of amyloid-related neurodegeneration.

Acknowledgements

The authors have benefited from useful access to the Hybrilit heterogeneous computing platform, which was kindly provided by MLIT JINR.

Conflicts of interest

No potential conflict of interest was reported by the authors.

Funding

The present work was supported by the JINR project "Nanobiophotonics" (# 1147-1).

Data availability statement

Data available on request from the authors.

References

[1] D. J. Selkoe, J. Hardy, The amyloid hypothesis of Alzheimer's disease at 25 years, EMBO Mol. Med. 8 (2016) 595.

[2] F. Chiti, C. M. Dobson, Protein misfolding, amyloid formation, and human disease: A summary of progress over the last decade, Ann. Rev. Biochem. 86 (2017) 27.

[3] N. G. Sgourakis, Y. Yan, S. A. McCallum, C. Wang, A. E. Garcia, The Alzheimer's peptides Abeta40 and 42 adopt distinct conformations in water: A combined MD/NMR study, J. Mol. Biol. 368 (2007) 1448.

[4] S. Chakraborty, P. Das, Emergence of alternative structures in amyloid beta 1–42 monomeric landscape by N-terminal hexapeptide amyloid inhibitors, Sci. Rep. 7 (2017) 9941.

[5] L. Tran, N. Basdevant, C. Prévost, T. Ha-Duong, Structure of ring-shaped Aβ42 oligomers determined by conformational selection, Sci. Rep. 6 (2016) 21429.

[6] S. De, D. C. Wirthensohn, P. Flagmeier, C. Hughes, F. A. Aprile, F. S. Ruggeri, D. R. Whiten, D. Emin, Z. Xia, J. A. Varela, P. Sormanni, F. Kundel, T. P. J. Knowles, C. M. Dobson, C. Bryant, M. Vendruscolo, D. Klenerman, Different soluble aggregates of Aβ42 can give rise to cellular toxicity through different mechanisms, Nat. Commun. 10 (2019) 1541.

[7] I. V. J. Murray, L. Liu, H. Komatsu, K. Uryu, G. Xiao, J. A. Lawson, P. H. Axelsen, Membrane-mediated amyloidogenesis and the promotion of oxidative lipid damage by amyloid beta proteins, J. Biol. Chem. 282 (2007) 9335.

[8] V. Corradi, B. I. Sejdiu, H. Mesa-Galloso, H. Abdizadeh, S. Y. Noskov, S. J. Marrink, D. P. Tieleman, Emerging diversity in lipid–protein interactions, Chem. Rev. 119 (2019) 5775.

[9] M. P. Muller, T. Jiang, C. Sun, M. Lihan, S. Pant, P. Mahinthichaichan, A. Trifan, E. Tajkhorshid, Characterization of lipid–protein interactions and lipid-mediated modulation of membrane protein function through molecular simulation, Chem. Rev. 119 (2019) 6086.

[10] S. Ciudad, E. Puig, T. Botzanowski, M. Meigooni, A. S. Arango, J. Do, M. Mayzel, M. Bayoumi, S. Chaignepain, G. Maglia, S. Cianferani, V. Orekhov, E. Tajkhorshid, B. Bardiaux, N. Carulla, Aβ(1–42) tetramer and octamer structures reveal edge conductivity pores as a mechanism for membrane damage, Nat. Commun. 11 (2020) 3014.

[11] M. F. M. Sciacca, C. La Rosa, D. Milardi, Amyloid-Mediated Mechanisms of Membrane Disruption, in: Biophysica, 2021, p. 137.

[12] O. Crescenzi, S. Tomaselli, R. Guerrini, S. Salvadori, A. M. D'Ursi, P. A. Temussi, D. Picone, Solution structure of the Alzheimer amyloid β-peptide (1–42) in an apolar microenvironment, Eur. J. Biochem. 269 (2002) 5642.

[13] T. R. Molugu, R. L. Thurmond, T. M. Alam, T. P. Trouard, M. F. Brown, Phospholipid headgroups govern area per lipid and emergent elastic properties of bilayers, Biophys. J. 121 (2022) 4205.

[14] P. Maleš, Z. Brkljača, I. Crnolatac, D. Petrov, D. Bakarić, Phase-dependent adsorption of myelin basic protein to phosphatidylcholine lipid bilayers, Membranes (Basel) 14 (2024).

[15] J. F. Nagle, S. Tristram-Nagle, Structure of lipid bilayers, Biochim. Biophys. Acta 1469 (2000) 159.

[16] W. Chen, F. Duša, J. Witos, S.-K. Ruokonen, S. K. Wiedmer, Determination of the main phase transition temperature of phospholipids by nanoplasmonic sensing, Sci. Rep. 8 (2018) 14815.

[17] N. Kučerka, M. P. Nieh, J. Katsaras, Fluid phase lipid areas and bilayer thicknesses of commonly used phosphatidylcholines as a function of temperature, Biochim. Biophys. Acta 1808 (2011) 2761.

[18] G. Neunert, J. Tomaszewska-Gras, A. Baj, M. Gauza-Włodarczyk, S. Witkowski, K. Polewski, Phase transitions and structural changes in DPPC liposomes induced by a 1-carba-alpha-tocopherol analogue, Molecules 26 (2021).

[19] R. N. Lewis, R. N. McElhaney, Fourier transform infrared spectroscopy in the study of lipid phase transitions in model and biological membranes: Practical considerations, Methods Mol. Biol. 400 (2007) 207.

[20] D. A. Pink, S. McNeil, B. Quinn, M. J. Zuckermann, A model of hydrogen bond formation in phosphatidylethanolamine bilayers, Biochim. Biophys. Acta 1368 (1998) 289.

[21] V. A. Lorenz-Fonfria, Infrared difference spectroscopy of proteins: From bands to bonds, Chem. Rev. 120 (2020) 3466.

[22] S. M. Kelly, T. J. Jess, N. C. Price, How to study proteins by circular dichroism, Biochim. Biophys. Acta 1751 (2005) 119.

[23] S. U. Sane, S. M. Cramer, T. M. Przybycien, A holistic approach to protein secondary structure characterization using Amide I band Raman spectroscopy, Anal. Biochem. 269 (1999) 255.

[24] N. J. Greenfield, Using circular dichroism spectra to estimate protein secondary structure, Nat. Protoc. 1 (2006) 2876.

[25] P. S. Kumagai, A. P. U. Araujo, J. L. S. Lopes, Going deep into protein secondary structure with synchrotron radiation circular dichroism spectroscopy, Biophys. Rev. 9 (2017) 517.

[26] Z. D. Schultz, I. W. Levin, Vibrational spectroscopy of biomembranes, Ann. Rev. Anal. Chem. (Palo Alto Calif) 4 (2011) 343.

[27] P. N. Jemmett, D. C. Milan, R. J. Nichols, T. Howitt, A. L. Martin, T. Arnold, J. L. Rawle, C. L. Nicklin, T. R. Dafforn, L. R. Cox, S. L. Horswell, Influence of the lipid backbone on electrochemical phase behavior, Langmuir 38 (2022) 14290.

[28] A. Botan, F. Favela-Rosales, P. F. J. Fuchs, M. Javanainen, M. Kanduč, W. Kulig, A. Lamberg, C. Loison, A. Lyubartsev, M. S. Miettinen, L. Monticelli, J. Määttä, O. H. S. Ollila, M. Retegan, T. Róg, H. Santuz, J. Tynkkynen, Toward atomistic resolution structure of phosphatidylcholine headgroup and glycerol backbone at different ambient conditions, J. Phys. Chem. B 119 (2015) 15075.

[29] J. A. Lemkul, D. R. Bevan, Destabilizing Alzheimer's beta(42) protofibrils with morin: Mechanistic insights from molecular dynamics simulations, Biochem. 49 (2010) 3935.

[30] N. Sreerama, R. W. Woody, A self-consistent method for the analysis of protein secondary structure from circular dichroism, Anal. Biochem. 209 (1993) 32.

[31] S. W. Provencher, J. Glöckner, Estimation of globular protein secondary structure from circular dichroism, Biochem. 20 (1981) 33.

[32] N. Sreerama, R. W. Woody, Estimation of protein secondary structure from circular dichroism spectra: Comparison of CONTIN, SELCON, and CDSSTR methods with an expanded reference set, Anal. Biochem. 287 (2000) 252.

[33] S. Jo, T. Kim, V. G. Iyer, W. Im, CHARMM-GUI: A web-based graphical user interface for CHARMM, J. Comput. Chem. 29 (2008) 1859.

[34] S. Tomaselli, V. Esposito, P. Vangone, N. A. J. van Nuland, A. M. J. J. Bonvin, R. Guerrini, T. Tancredi, P. A. Temussi, D. Picone, The α-to-β conformational transition of Alzheimer's Aβ-(1–42) peptide in aqueous media is reversible: A step by step conformational analysis suggests the location of β conformation seeding, ChemBioChem 7 (2006) 257.

[35] W. L. Jorgensen, J. Chandrasekhar, J. D. Madura, R. W. Impey, M. L. Klein, Comparison of simple potential functions for simulating liquid water, J. Chem. Phys. 79 (1983) 926.

[36] J. Huang, A. D. MacKerell, Jr. CHARMM36 all-atom additive protein force field: Validation based on comparison to NMR data, J. Comput. Chem. 34 (2013) 2135.

[37] K. A. A. Abdeljawaad, Y. Arynbek, K. Mamatkulov, H. Duc Le, M. A. A. Ibrahim, G. A. H. Mekhemer, G. Arzumanyan, pH modulates amyloid-β42 conformation in lipid membranes: Evidence from circular dichroism, Raman spectroscopy, and molecular dynamics simulations, J. Biomol. Struct. Dyn. (2025) 1.

[38] M. J. Abraham, T. Murtola, R. Schulz, S. Páll, J. C. Smith, B. Hess, E. Lindahl, GROMACS: High performance molecular simulations through multi-level parallelism from laptops to supercomputers, SoftwareX 1–2 (2015) 19.

[39] M. Parrinello, A. Rahman, Polymorphic transitions in single crystals: A new molecular dynamics method, J. Appl. Phys. 52 (1981) 7182.

[40] T. Darden, D. York, L. Pedersen, Particle mesh Ewald: An $N \cdot \log(N)$ method for Ewald sums in large systems, J. Chem. Phys. 98 (1993) 10089.

[41] W. Humphrey, A. Dalke, K. Schulten, VMD: Visual molecular dynamics, J. Mol. Graph. 14 (1996) 33.

[42] S. Zavatski, H. Bandarenka, Ł. Hetmańczyk, J. Hetmańczyk, M. Vorobyeva, Y. Arynbek, K. Mamatkulov, G. Arzumanyan, Model phospholipid interaction with cholesterol and melatonin: Raman spectroscopy and density functional theory study, J. Raman Spectrosc. 53 (2022) 1540.

[43] S. Kint, P. H. Wermer, J. R. Scherer, Raman spectra of hydrated phospholipid bilayers. 2. Water and head-group interactions, J. Phys. Chem. 96 (1992) 446.

[44] A. Lörincz, J. Mihály, C. Németh, A. Wacha, A. Bóta, A. Effects of ursolic acid on the structural and morphological behaviours of dipalmitoyl lecithin vesicles, Biochim. Biophys. Acta (BBA) — Biomembr. 1848 (2015) 1092.

[45] A. Fasanella, K. Cosentino, A. Beneduci, G. Chidichimo, E. Cazzanelli, R. C. Barberi, M. Castriota, Thermal structural evolutions of DMPC-water biomimetic systems investigated by Raman spectroscopy, Biochim. Biophys. Acta (BBA) — Biomembr. 1860 (2018) 1253.

[46] R. Gharib, A. Najjar, L. Auezova, C. Charcosset, H. Greige-Gerges, Interaction of selected phenylpropenes with dipalmitoylphosphatidylcholine membrane and their relevance to antibacterial activity, J. Membr. Biol. 250 (2017) 259.

[47] T. Kondela, E. Dushanov, M. Vorobyeva, K. Mamatkulov, E. Drolle, D. Soloviov, P. Hrubovčák, K. Kholmurodov, G. Arzumanyan, Z. Leonenko, N. Kučerka, Investigating the competitive effects of cholesterol and melatonin in model lipid membranes, Biochim. Biophys. Acta (BBA) — Biomembr. 1863 (2021) 183651.

[48] Y. V. Zaytseva, S. V. Adichtchev, N. V. Surovtsev, Raman study of temperature-induced hydrocarbon chain disorder in saturated phosphatidylcholines, Chem. Phys. Lipids 230 (2020) 104926.

[49] R. N. A. H. Lewis, R. N. McElhaney, Membrane lipid phase transitions and phase organization studied by Fourier transform infrared spectroscopy, Biochim. Biophys. Acta (BBA) — Biomembr. 1828 (2013) 2347.

[50] S. Kurakin, D. Badreeva, E. Dushanov, A. Shutikov, S. Efimov, A. Timerova, T. Mukhametzyanov, T. Murugova, O. Ivankov, K. Mamatkulov, G. Arzumanyan, V. Klochkov, N. Kučerka, Arrangement of lipid vesicles and bicelle-like structures formed in the presence of Aβ(25–35) peptide, Biochim. Biophys. Acta (BBA) — Biomembr. 1866 (2024) 184237.

[51] Z. Movasaghi, S. Rehman, I. U. Rehman, Raman spectroscopy of biological tissues, Appl. Spectrosc. Rev. 42 (2007) 493.

[52] A. V. Veluthandath, W. Ahmed, J. Madsen, H. W. Clark, A. D. Postle, J. S. Wilkinson, G. S. Murugan, Quantification of lung surfactant lipid (dipalmitoylphosphatidylcholine/sphingomyelin) ratio in binary liposomes using Raman spectroscopy, J. Raman Spectrosc. 55 (2024) 386.

[53] H. A. Esawii, K. Mamatkulov, H. A. Mahran, G. Arzumanyan, N. Mohamed, Investigation into Alzheimer's-related amyloid-β conformational transformations and stability influenced by green iron oxide nanoparticles (GIONP), Intern. J. Biol. Macromol. 298 (2025) 140124.

[54] S. Rivas-Arancibia, E. Rodriguez-Martinez, I. Badillo-Ramirez, U. Lopez-Gonzalez, J. M. Saniger, Structural changes of amyloid beta in hippocampus of rats exposed to ozone: A Raman spectroscopy study, Front. Mol. Neurosci. 10 (2017) 137.

[55] C. Mensch, P. Bultinck, C. Johannessen, The effect of protein backbone hydration on the amide vibrations in Raman and Raman optical activity spectra, Phys. Chem. Chem. Phys. 21 (2019) 1988.

[56] S. Ramos, J. C. Lee, Raman spectroscopy in the study of amyloid formation and phase separation, Biochem. Soc. Trans. 52 (2024) 1121.

[57] S.-Y. Lin, H.-L. Chu, H.-L. Wei, Secondary conformations and temperature effect on structural transformation of amyloid β(1–28), (1–40) and (1–42) peptides, J. Biomol. Struct. Dyn. 20 (2003) 595.

[58] N. C. Maiti, M. M. Apetri, M. G. Zagorski, P. R. Carey, V. E. Anderson, Raman spectroscopic characterization of secondary structure in natively unfolded proteins: α-synuclein, J. Am. Chem. Soc. 126 (2004) 2399.

[59] A. Sadat, I. J. Joye, Peak Fitting Applied to Fourier transform infrared and Raman spectroscopic analysis of proteins, in: Appl. Sci., 2020.

[60] S. Ngarize, H. Herman, A. Adams, N. Howell, Comparison of changes in the secondary structure of unheated, heated, and high-pressure-treated β-lactoglobulin and qvalbumin proteins using Fourier transform Raman spectroscopy and self-deconvolution, J. Agric. Food Chem. 51 (2004) 6470.

[61] F. Tofoleanu, N.-V. Buchete, Alzheimer Aβ peptide interactions with lipid membranes, Prion 6 (2012) 339.

[62] H. Ahyayauch, M. E. Masserini, A. Alonso, F. M. Goñi, Understanding Aβ peptide binding to lipid membranes: A biophysical perspective, in: Intern. J. Mol. Sci., 2024.

[63] M. Yang, K. Wang, J. Lin, L. Wang, F. Wei, J. Zhu, W. Zheng, L. Shen, Gel phase membrane retards amyloid β-peptide (1–42) fibrillation by restricting slaved diffusion of peptides on lipid bilayers, Langmuir 34 (2018) 8408.

[64] C. Poojari, A. Kukol, B. Strodel, How the amyloid-β peptide and membranes affect each other: An extensive simulation study, Biochim. Biophys. Acta (BBA) — Biomembr. 1828 (2013) 327.

[65] B. Shivu, S. Seshadri, J. Li, K. A. Oberg, V. N. Uversky, A. L. Fink, Distinct β-sheet structure in protein aggregates determined by ATR–FTIR spectroscopy, Biochem. 52 (2013) 5176.

[66] M. Suzuki, T. Miura, Effect of amyloid β-peptide on the fluidity of phosphatidylcholine membranes: Uses and limitations of diphenylhexatriene fluorescence anisotropy, Biochim. Biophys. Acta (BBA) — Biomembr. 1848 (2015) 753.

[67] M. Inayathullah, D. B. Teplow, Structural dynamics of the ΔE22 (Osaka) familial Alzheimer's disease-linked amyloid β-protein, Amyloid 18 (2011) 98.

[68] M. Suzuki, T. Miura, Effect of amyloid β-peptide on the fluidity of phosphatidylcholine membranes: Uses and limitations of diphenylhexatriene fluorescence anisotropy, Biochim. Biophys. Acta 1848 (2015) 753.